



Full paper



# Magnetic-interaction assisted hybridized triboelectric-electromagnetic nanogenerator for advanced human-machine interfaces

Long Liu<sup>a,b,c,d</sup>, Qiongfeng Shi<sup>a,b,c,d</sup>, Zhongda Sun<sup>a,b,c,d</sup>, Chengkuo Lee<sup>a,b,c,d,e,\*</sup>

<sup>a</sup> Department of Electrical and Computer Engineering, National University of Singapore, 4 Engineering Drive 3, 117576, Singapore

<sup>b</sup> Center for Intelligent Sensors and MEMS, National University of Singapore, Block E6 #05-11, 5 Engineering Drive 1, 117608, Singapore

<sup>c</sup> Hybrid-Integrated Flexible (Stretchable) Electronic Systems Program (HIFES), National University of Singapore, Block E6 #05-3, 5 Engineering Drive 1, 117608, Singapore

<sup>d</sup> NUS Suzhou Research Institute (NUSRI), Suzhou Industrial Park, Suzhou 215123, PR China

<sup>e</sup> NUS Graduate School - Integrative Sciences and Engineering Programme (ISEP), National University of Singapore, 119077, Singapore

## ARTICLE INFO

### Keywords:

Hybridized triboelectric-electromagnetic nanogenerator  
Magnetic attraction  
Internet of things  
Human-machine interface

## ABSTRACT

A magnetic-interaction assisted hybridized triboelectric-electromagnetic nanogenerator (MAHN) is designed and optimized with two magnets in attraction, and a silicone-based cushion with microstructures. The whole device including a fixed part and a moving part has a small size of 35 mm × 35 mm × 8 mm. After various energy harvesting and sensing characterizations, the MAHN has been verified as an efficient energy harvester, as well as a self-powered sensor for advanced human-computer interface (HMI). For energy harvesting, the triboelectric nanogenerator (TENG) delivers a peak power of 6.89 mW at the load of 1.1 MΩ, and the electromagnetic generator (EMG) delivers a peak power of 2.7 mW at the load of 1.1 kΩ. With the hybridized buck circuit, outputs from both the TENG and the EMG can be rectified and integrated efficiently to charge capacitors. A capacitor of 100 μF is charged to 2.03 V within 30 s, which is better than the performances of individual generators and their parallel-connection with only rectifiers. A thermometer and a Bluetooth module are powered with different amounts of the attracted magnet, implying the wide adaptability of the MAHN. Advanced applications of HMI have also been developed with cross-divided electrodes in the MAHN, such as orientation control in a game of Snake, real-time operation of a PowerPoint presentation, and recognition of simple air gestures in contactless control. Moreover, a 3 × 3 array is prepared and signal channels are simplified by traversal method without loss of functions to achieve higher-level control. A virtual football game is demonstrated by a shoe moving on the array, and different kinds of shootings have been mapped to the player in the game.

## 1. Introduction

With the rapid development of the Internet of Things (IoT), vastly distributed devices are playing important roles in the areas of environmental monitoring, healthcare, and smart home, etc [1,2]. To address the power challenges of numerous devices with abundant functional sensors nowadays, various energy harvesting technologies including triboelectric nanogenerator (TENG) [3–7], electromagnetic generator (EMG) [8], and piezoelectric nanogenerator (PENG) [9], are introduced to convert irregular mechanical energy into electric power. Thereinto, the TENG has been extensively studied with different mechanical sources like rotation [10–12], vibration [13–15], human motion [16–18], and water wave [19–21], and proved to be effective power

supplies with advantages of high output, easy fabrication and low cost. However, hybridized mechanism of combining TENG with other energy harvesting technologies like piezoelectric [22–24], electromagnetic [25–37], and solar cells [38–41], is still required in the prototype to provide sufficient power and adapt various kinds of operations.

The hybridized triboelectric-electromagnetic nanogenerator is one of the largest branches among hybridized devices [42–44]. The structure design of hybridized triboelectric-electromagnetic nanogenerator can be roughly divided into two types: contact-separation type based on contact-separation mode TENG [25–28], and sliding/rotating type based on the sliding-mode/freestanding-mode TENG [34–37]. Conventionally, a single unit of the EMG possesses one magnet. Recently, multiple magnets have been applied to achieve dynamic equilibrium of

\* Corresponding author at: Department of Electrical and Computer Engineering, National University of Singapore, 4 Engineering Drive 3, Singapore 117576, Singapore.

E-mail address: [elelc@nus.edu.sg](mailto:elelc@nus.edu.sg) (C. Lee).

<https://doi.org/10.1016/j.nanoen.2021.106154>

Received 20 February 2021; Received in revised form 13 April 2021; Accepted 7 May 2021

Available online 13 May 2021

2211-2855/© 2021 Elsevier Ltd. All rights reserved.

the movable magnet in its balance state in harvesting low-frequency mechanical energy. For example, Seol et al. proposed an oscillating magnet suspended in the tube by dual-directional magnetic repulsive forces, which enabled versatile energy harvesting capability at frequencies in the sub-10 Hz range [45]. Additionally, Shao et al. introduced magnet pairs that produce attractions to achieve contact-separation mode TENGs and rotary freestanding-mode EMGs in harvesting blue energy [46]. Although with multiple magnets structure, mechanical equilibrium of the movable magnet can be achieved, yet this inevitably increases the overall system complexity. Theoretically, multiple magnets can produce a higher electromagnetic field which has a great potential to enhance the output performance of the EMG, but the influence of multiple magnets on the output performance is rarely studied in the literature.

Although the hybridized triboelectric-electromagnetic nanogenerators have been reported a lot, most works are focusing on energy harvesting rather than applying in advanced human-machine interfaces (HMIs) [47]. As for the HMIs, three mainstream applications have been developed by a large amount of wearable/portable devices, such as controlling the robotic arm with wearable patches [48,49], driving the drone with tactile devices [50], and playing VR/AR game with gloves [51]. Reported hybridized triboelectric-electromagnetic nanogenerators as shown in Table S1 have been demonstrated for various sensing applications, show potential for realizing the above applications about HMIs. Chen et al. proposed a hybridized triboelectric-electromagnetic nanogenerator based on freestanding magnet moving in-plane arbitrarily [52]. However, only triboelectric signals are utilized when the prepared device is applied as a vibration sensor in playing the "HitHamster" game. Furthermore, Wan et al. developed an array of flexible hybridized electromagnetic-triboelectric nanogenerators for 3D trajectory sensing by a magnetic part attached on a finger crossing over the copper FPCB coil array [53], while only electromagnetic signals obtained from the integrated coil array are utilized for sensing. Most recently, Bhatta et al. prepared a magnetic repulsion-assisted hybrid nanogenerator [54]. A central magnet can drive the side magnet aligned in the same magnetization direction moving, resulting in only electromagnetic signals are applied for detecting the motion parameters along with in-plane arbitrary directions. The synergistically integrated hybridized mechanism can provide more flexibility in HMI design, more diverse controllable signals, and higher degrees of freedom in operations, but few works illustrate using both triboelectric signals and electromagnetic signals in HMI applications.

Herein, a magnetic-interaction assisted hybridized triboelectric-electromagnetic nanogenerator (MAHN) is designed with one moving part and one fixed part, where a pair of attracted magnets (Diameter 30 mm, Thickness 2 mm) are embedded in each part and the whole device is with a small size of 35 mm  $\times$  35 mm  $\times$  8 mm. So that, the TENG and the EMG can simultaneously convert the mechanical energy of impacts into electric power as two parts attracting to each other during contact-separation processes. Outputs of the TENG and the EMG have been enhanced by the powerful attraction, and the scaling-down effect of output performance by lower operating frequency has been weakened with magnetic attraction induced by the two-magnet design. The MAHN has been proved as an efficient energy harvester working with hybridized buck convert circuit, which is better than the performances of individual and parallel-connection. Attributed to the adaptivity of magnets' amount, the MAHN is applied as an adjustable energy harvester in powering different electronics. By utilizing both the triboelectric signals and electromagnetic signals, the MAHN can function as an advanced HMI in entertainment, office, and gaming control, providing higher controlling capability and flexibility in various scenarios. Moreover, non-contact operations have been developed by the user waves the vertical moving part above the fixed part, resulting in recognizing simple air gestures for contactless controlling. Finally, the 3  $\times$  3 array of the MAHN is prepared and channels are simplified by traversal method without loss of functions. And a virtual football game is

demonstrated with the user moving the shoe on the array, assisting the player in the game in locating at different zones and shooting in different directions. To sum up, the MAHN can be applied as an efficient energy harvester, as well as an advanced human-machine interface in various practical scenarios.

## 2. Results and discussion

### 2.1. Design and optimization of the MAHN as a hybridized energy harvester

The MAHN is schematically presented in Fig. 1, in which the moving part and the fixed part are marked with two braces. As shown in Fig. 1a, a pair of magnets are placed inside two parts respectively. The magnetization direction is along the thickness direction, and magnet poles are opposite in confronting faces of two magnets. Due to magnetic attraction, two parts of the MAHN are attached at the rest state, as shown in Fig. 1b. The device in attraction presents a dimension of 35 mm  $\times$  35 mm  $\times$  8 mm, which is easily separated by manual operations, and two parts in the discrete state are shown in Fig. 1c. The fixed part has a thickness of 4.5 mm, and multi wires are led out from this part for applications in energy harvesting and self-powered sensing. The moving part has a thickness of 3.5 mm and is applied as an independent part without leading wires. A promising application scenario is also shown in Fig. 1a, where the moving part of the MAHN is operated with the user's hand, and the fixed part is attached on the podium for connecting external load. After operations of contact mode and no-contact mode, the user can put the moving part back and locate it on the fixed part.

Through a COMSOL simulation shown in Fig. 1d, magnetic induction lines are gathered in between two magnets in attraction. Based on this gathering trend, the output of EMG can be enhanced due to more intensive magnetic flux through the coil when compared with the simulation in Fig. S1. To verify the simulation, comparison tests between two magnets in attraction and a single magnet are carried with the force gauge (Mecmesin, MultiTest 2.5-i) to remove most of the uncertainties from manual operation, where the instrument is moving at the largest speed of 900 mm/min. The results shown in Fig. S2 have proved that the output voltage of the coil in fixed part increases by introduced another magnet under the coil, which is in accord with the simulation.

Moreover, the effect of the cushion is also explored with the force gauge, and results are shown in Fig. S3. The cushion in the MAHN is designed by curing Eco-flex rubber on a conductive textile. The braided structure is applied as a mold for fabricating the microstructure on the cushion's bottom surface. After demolding from the conductive textile, obvious microstructures have been obtained and shown in Fig. S3c, which is similar to the braided structure shown in Fig. S3b. The microstructure helps the cushion recover from the bottom contact surface after impact, rather than stick on the bottom contact surface. As shown in Fig. S3a, increasing output voltage of different TENGs defined as D1 (Single magnet & Without cushion), D2 (Two magnets in attraction & Without cushion), D3 (Two magnets in attraction & Cushion without microstructure), D4 (Two magnets in attraction & Cushion with microstructure), have proved the positive effect of magnetic attraction for close contact and designed cushion for increasing contact surface area. Through the above discussion, introduced magnetic attraction has both improved performance of the TENG and the EMG in the MAHN.

In Fig. 2, the working principle and output performance have been further discussed. As a lateral view shown in Fig. 2a, The MAHN is based on contact-separation structured TENG and EMG. An intact square electrode is utilized in TENG to apply as a hybridized energy harvester in Fig. 2a. At rest state, the moving part and the fixed part are attracted to each other, where charge balance is achieved among contact interface. According to the triboelectric series, the FEP layer generates negative charges to maintain a neutralization with a positively charged Al layer in the moving part. Due to the cushion's microstructure rubbing with the bottom interface, a small number of negative charges generated in the

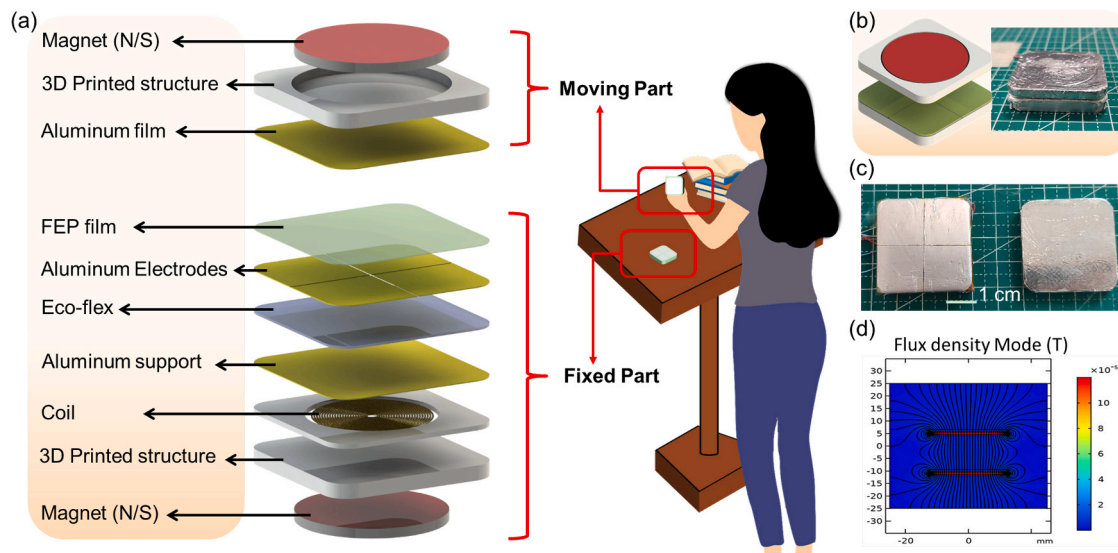


**Fig. 1.** (a) Schematic diagram of the magnetic-interaction assisted hybridized triboelectric-electromagnetic nanogenerator (MAHN). (b) Photo of the prepared device in the rest state. (c) Photo of the prepared device in the discrete state. (d) Simulated distribution of the magnetic field of two magnets in attraction.

cushion area also contributes to charge balance, which is marked in red and compatible with the comparison result in Fig. S2. On the other hand, there is no current flow in the coil of the EMG under rest state. Next, when the moving part is separating from the fixed part with external force overcoming magnetic attraction, the charge balance is broken, and the magnetic flux crossing the coil decreases. As a result, positive charges flow from the ground to TENG's electrode, an induced current is generated in the coil. On the contrary, positive charges will flow from TENG's electrode to the ground when the moving part is approaching and attracted to the fixed part, as while an induced current in the opposite direction is generated in the coil due to increasing magnetic flux. It should be noted that approaching actions are converted into impacts eventually as the moving part in the magnetic attraction range.

From the above analysis, the TENG and EMG in the MAHN are cooperatively working along with the contact-separation processes. The outputs are measured with a multichannel oscilloscope, where leading wires from the fixed part are connected and tested simultaneously. The distance apart is controlled within 2 cm, and the frequency of the manual impact is changed according to a metronome. As shown in Fig. 2b, there are positive peaks obtained during impacts and negative peaks during separations. Meanwhile, both voltages and currents of impacts are higher than those of separation, either for the TENG or the EMG. Through tests under different frequencies, the TENG has presented an average output voltage of 280.7 V at 0.5 Hz, 296.8 V at 1 Hz, 309.4 V at 2 Hz, 339.0 V at 3 Hz, and 369.2 V at 4 Hz. In contrast, the EMG has delivered an average output voltage of 1.04 V at 0.5 Hz, 1.26 V at 1 Hz, 1.44 V at 2 Hz, 1.59 V at 3 Hz, 1.87 V at 4 Hz. As a result, even when the operating frequency decreases from 4 Hz to 0.5 Hz, the output voltage of the TENG can still maintain 76% while that of the EMG can maintain 56%. Output currents have also been tested in different frequencies, where average currents of the TENG reach 6.7  $\mu$ A at 0.5 Hz, 7.4  $\mu$ A at 1 Hz, 8.5  $\mu$ A at 2 Hz, 8.71  $\mu$ A at 3 Hz, and 9.9  $\mu$ A at 4 Hz, average currents of the EMG reach 0.73 mA at 0.5 Hz, 0.79 mA at 1 Hz, 0.89 mA at 2 Hz, 0.81 mA at 3 Hz, 0.95 mA at 4 Hz. The outputs have presented the trend of increasing as the operating frequency is increased. When the operating frequency decreases from 4 Hz to 0.5 Hz, the output current of the TENG can maintain 68% while that of the EMG can maintain 77%. It is worth mentioning that the outputs of the TENG and the EMG are increased when the distance apart of manual impacts are not limited, as shown in Fig. S4.

The above analysis is based on the moving part is unfixed. In contrast, when the moving part is fixed on a linear motor to exclude

influences of the magnetic attraction and changed operation distance, the results have demonstrated increased trends in Fig. S5. Both the TENG and the EMG present increase trends as frequency increases, either voltages or currents. But all the output values are lower than those under manual operations with the unfixed moving part. After calculation, when the operating frequency decreases from 4 Hz to 0.5 Hz, the output current of the TENG can only maintain 16% while that of the EMG can maintain 13%. And output current of the TENG can only maintain 13% from 4 Hz to 0.5 Hz, while the output current of the EMG has reduced by 14% from 4 Hz to 0.5 Hz. By comparison, the manual operations of the split design (one moving part and one fixed part) in the MAHN have weakened the scaling-down effect of output performance by lower operating frequency, due to the magnetic attraction which can help improve output performances. In brief, results have demonstrated the adaptability of the MAHN as an efficient hybridized energy harvester for impact energy under different operating frequencies.

To evaluate the performance of the MAHN as a hybridized energy harvester, output power and capacitor charging have been tested in Fig. 3. First, a series of resistors have been parallel-connected with the TENG and the EMG, and corresponding voltages are tested for calculating output power. As shown in Fig. 3a, the output voltage of the TENG increases from 0.78 V to 179.6 V with the increasing value of the external loading resistance from 10 k $\Omega$  to 100 M $\Omega$ . Through calculation, maximum peak power has reached 6.89 mW at the load of 1.1 M $\Omega$ . Similar to Fig. 3b, the output voltage of the EMG increases from 0.03 V to 3.25 V by increasing external loading resistance from 10  $\Omega$  to 100 k $\Omega$ . And maximum peak power has reached 2.7 mW at the load of 1.1 k $\Omega$ . Take into consideration that the MAHN is small-sized (35 mm  $\times$  35 mm  $\times$  8 mm) and light-weight (33.1 g), the TENG has a maximum power density of 208.2 mW/Kg and the EMG has a maximum power density of 81.6 mW/Kg. Moreover, different capacitors are charged with individual energy harvesting parts and the hybridized device. As shown in Fig. 3d, capacitors of 1  $\mu$ F, 4.7  $\mu$ F, 10  $\mu$ F, and 47  $\mu$ F have been respectively charged to 3.15 V, 0.94 V, 0.56 V, and 0.11 V within 30 s with the rectified TENG under manual impacts of 2 Hz. On the other hand, capacitors of 1  $\mu$ F, 4.7  $\mu$ F, 10  $\mu$ F, 47  $\mu$ F, and 100  $\mu$ F have been respectively charged to 3.49 V, 3.24 V, 2.85 V, 2.18 V, and 1.61 V within 30 s with the rectified EMG in the same situation, which is shown in Fig. 3e. Moreover, the rectifier circuit shown in Fig. 3c is applied to integrate two energy harvesting units with the parallel connection. As result, capacitors of 1  $\mu$ F, 4.7  $\mu$ F, 10  $\mu$ F, 47  $\mu$ F, and 100  $\mu$ F have been respectively charged to 5.48 V, 3.99 V, 3.74 V, 2.63 V, and 1.63 V within 30 s in the

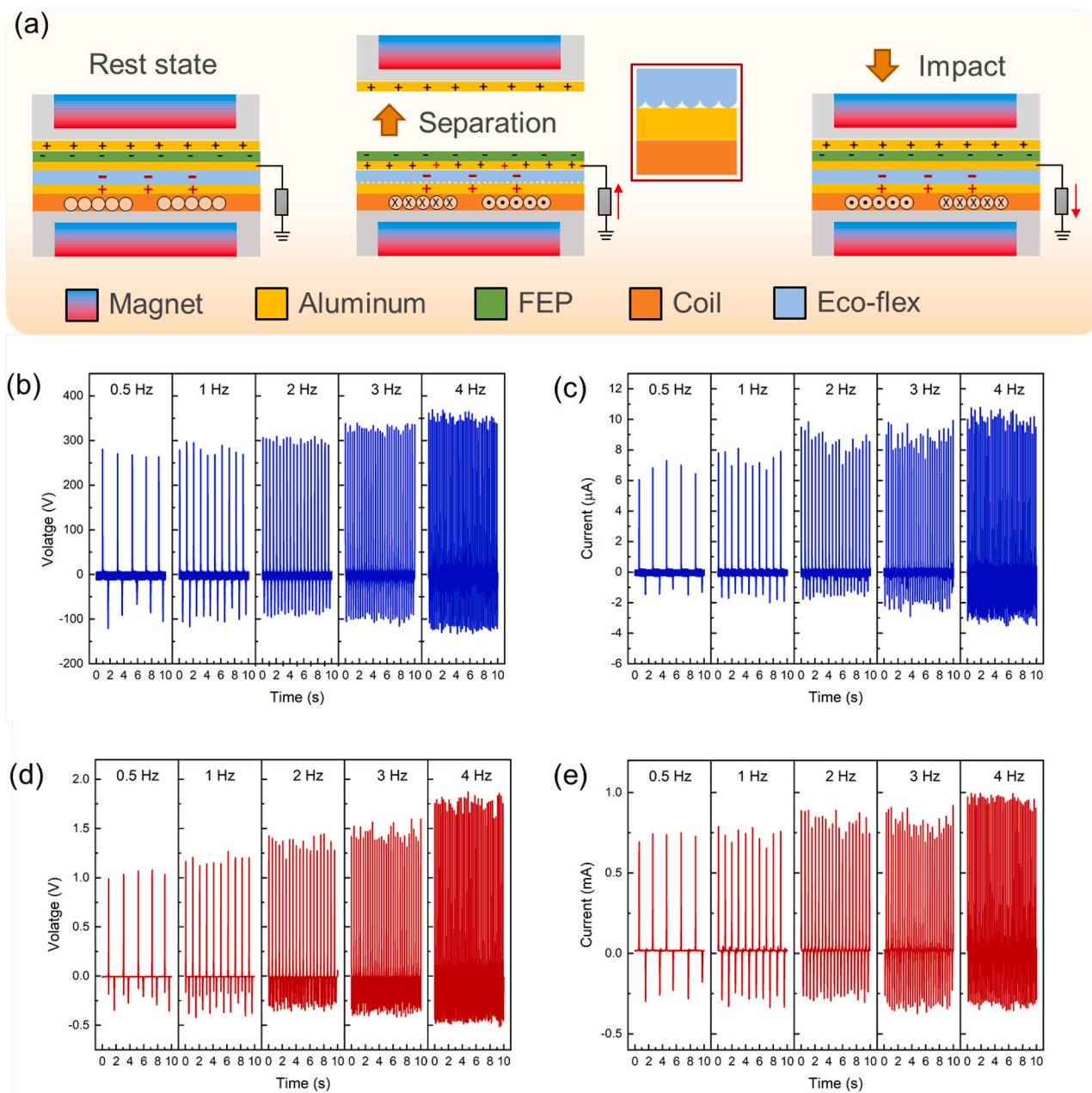


Fig. 2. (a) Working principle of the MAHN. (b) The output voltage of the TENG under contact-separation operations of different frequencies. (c) The output current of the TENG under contact-separation operations of different frequencies. (d) The output voltage of the EMG under contact-separation operations of different frequencies. (e) The output current of the EMG under contact-separation operations of different frequencies.

same situation, which is better than charged with the individual unit.

Although rectifiers in the parallel circuit have decreased the interaction effect of the TENG and the EMG, the hybridized buck circuit can further improve charging performance as shown in Fig. 4. Xi et.al, and Liang et.al have proved that the buck circuit is a universal power management strategy for TENG, in which the inductor is applied to absorb and store a part of the energy as the magnetic field energy [55–57]. Based on enlarged output signals of the TENG and the EMG shown in Fig. S6, the impact process has contributed a large part in outputs. With the induction coil of the EMG applied in the hybridized buck circuit, outputs in impact processes are integrated with rectified TENG signals, and a detailed design is shown in Fig. 4a. Results of charging performance are shown in Fig. 4b, capacitors of 1 μF, 4.7 μF, 10 μF, 47 μF, and 100 μF have been respectively charged to 7.54 V, 5.53 V, 4.25 V, 2.98 V and 2.03 V within 30 s with the hybridized buck

circuit, which is better than performances of individual and parallel connection. With the charging capacitor of 100 μF, a thermometer is successfully powered in Fig. 4d and Movie V1. That capacitor is firstly charged to 1.62 V then connected with the thermometer and displayed temperature on-screen has proved the MAHN as an efficient hybridized energy harvester.

Supplementary material related to this article can be found online at [doi:10.1016/j.nanoen.2021.106154](https://doi.org/10.1016/j.nanoen.2021.106154).

Owing to the discrete design of the moving part, the MAHN also present adaptability of hybridized energy harvester by changing the amount of magnet. The 3D printed structure of the moving part is also adapted to different requirements by changing dimensions. As shown in Figs. 4c, 3D printed structures have been adjusted to add more circular magnets, and the charging performances of two magnets and three magnets are tested with a capacitor of 100 μF. Results have shown that

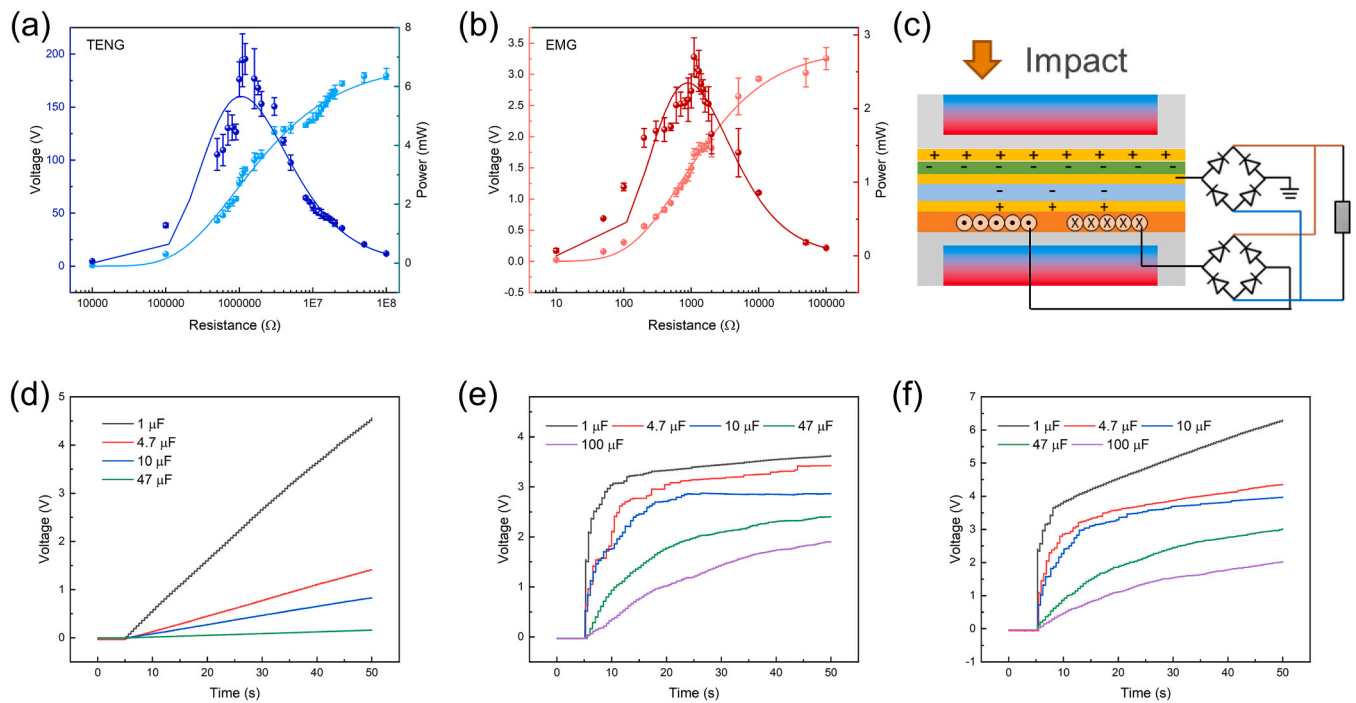


**Fig. 3.** (a) Resistance dependence of the voltage and peak output power of the TENG. (b) Resistance dependence of the voltage and peak output power of the EMG. (c) Rectified circuit of the TENG and the EMG in parallel connection. (d) Charging different capacitors with the TENG with manual impacts of 2 Hz. (e) Charging different capacitors with the EMG with manual impacts of 2 Hz. (f) Charging different capacitors with the parallel circuit with manual impacts of 2 Hz.

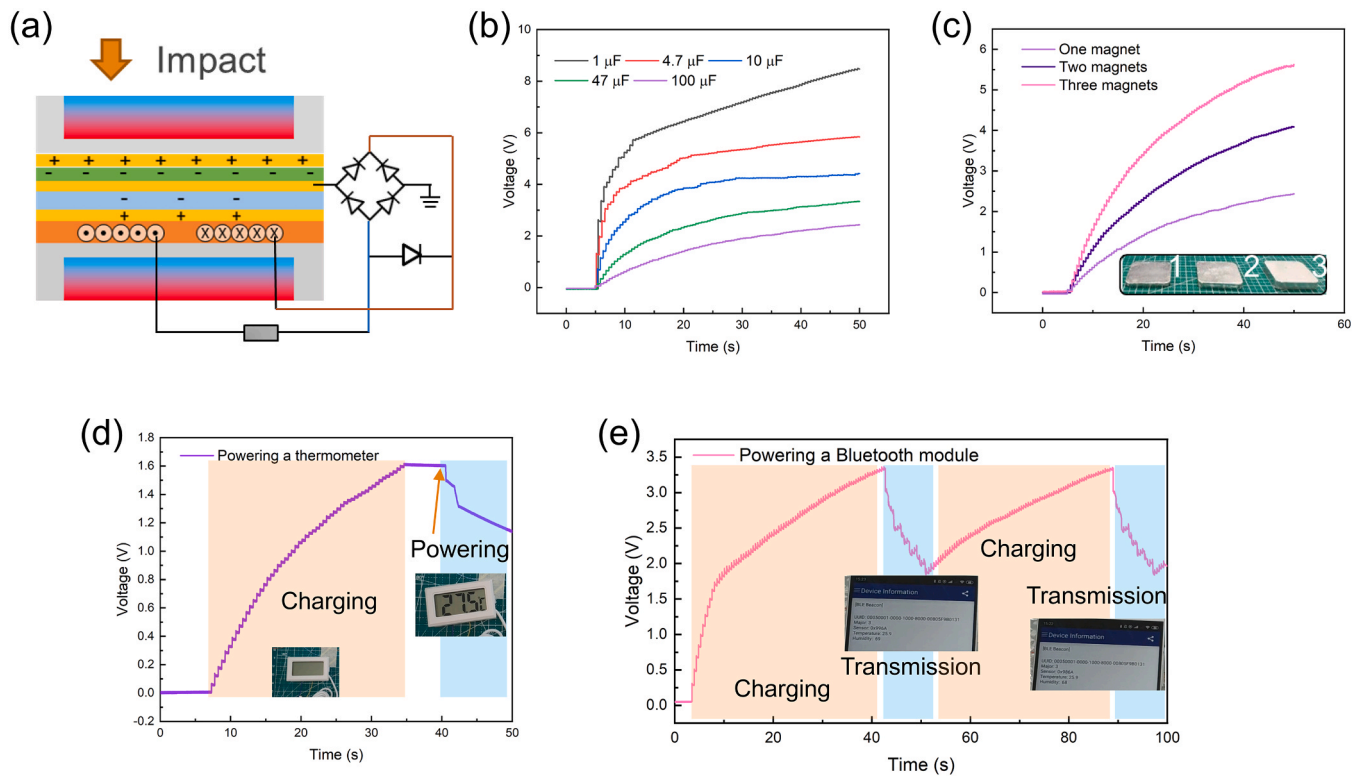


**Fig. 4.** (a) Hybridized buck circuit designed for the MAHN. (b) Charging different capacitors with the hybridized buck circuit with manual impacts of 2 Hz. (c) Charging a capacitor of 100  $\mu$ F with different amounts of magnets in the moving part of the MAHN. (d) Powering a thermometer. (e) Powering a Bluetooth module.

capacitor can be charged to 3.51 V by two magnets within 30 s with manual impacts of 2 Hz, and 4.89 V by three magnets in the same situation. Therefore, a Bluetooth module is successfully powered with an adapted moving part that contains three magnets. As shown in Fig. 4e

and Movie V2, the capacitor of 100  $\mu$ F has been charged to 3.34 V while directly connecting to the Bluetooth module. Thus, the module starts working and transferring signals of humidity and temperature to a terminal of a mobile phone. Along with continuous manual impacts, the

Bluetooth module can work again as the capacitor is charged to 3.34 V. Briefly, the MAHN can be an efficient energy harvester for impact energy and shows the promising potential of applying in scenarios where exists separated parts irregularly impacting each other, such as door's opening and closing belong to the smart home, and buffer structures in bridges belong to the smart traffic.

Supplementary material related to this article can be found online at [doi:10.1016/j.nanoen.2021.106154](https://doi.org/10.1016/j.nanoen.2021.106154).

## 2.2. Design and analysis of the MAHN as a self-powered sensor for advanced human-machine interface

Due to the design of magnetic attraction, the MAHN at the rest state presents a similar feature in the joystick for homing after transfer commands of direction. The intact triboelectric electrode in the fixed part can be crossed cut into four electrodes as shown in Fig. 1. A lateral view is shown in Fig. 5 to illustrate the working principle of the MAHN applied as a self-powered sensor in transferring commands of direction. At rest state, four electrodes are covered with the Al layer in the moving part, thus four single-electrode-based sliding TENGs have been formed. In Fig. 5a, two TENGs are displayed in view to explain the working principle, in which the charge balance is achieved referred to Fig. 2. When the moving part deviates from the rest position and slides to the left side, the negative charges in the FEP layer will lead to a change number of induced charges on two electrodes. As a result, positive charges flow from the left electrode to the ground and flow from the ground to the right electrode. When the moving part returns to the rest position, reverse signals are generated in two electrodes. Based on this working principle, four electrodes in the fixed part are designed and named as A1, A2, A3, and A4 in Fig. 5b. Designed operations are demonstrated in Movie V3. When the moving part of the MAHN moves along the directions of up, down, left, and right, four electrodes will generate signals according to the principle in Fig. 5a. As shown in Fig. 5c, four electrodes are tested with a multichannel oscilloscope,

simultaneously, and directions of up, down, left, and right can be easily determined by observing peaks among four electrodes. Obtained output voltages are within the range of  $-30\sim30$  V, changes in values of four electrodes are due to external press and release from handlers. When the moving part slides up and away from A3 and A4, there will be detected positive peaks in A1 and A2, while negative peaks in A3 and A4. In contrast, there will be negative peaks in A1 and A2 while positive peaks in A3 and A4 when the moving part slides down. The motions of left and right can be done in the same manner by determining which pair of electrodes are detected positive and which pair of electrodes are detected negative.

Supplementary material related to this article can be found online at [doi:10.1016/j.nanoen.2021.106154](https://doi.org/10.1016/j.nanoen.2021.106154).

Primary data collected from the oscilloscope have proved to distinguish moving directions of the moving part. To demonstrate the MAHN as an advanced human-machine interface, another open-source electronics platform of Arduino 2650 and match circuit are applied to read voltage signals in four electrodes. Signals read by Arduino board are illustrated in Fig. S7, in which four kinds of operations are identified with different changes. Moreover, a classical game of "Snake" is developed with Python code in Fig. 5d and Movie V4, in which the user can control directions of the Snake to eat randomly distributed food displayed on a computer. In Fig. S8, the interactions of the MAHN applying in the HMI are clarified. The Arduino board can read the first peaks of electrodes, and find out which two electrodes present positive peaks. Then the Arduino sends command codes of up, down, left, or right, into the Python code, and eventually changes the motions of the Snake. To sum up, the MAHN has been played as a self-powered "Joystick" in this application of entertainment, and the moving part will back to the rest position with help of magnetic attraction after transferring commands of directions.

Supplementary material related to this article can be found online at [doi:10.1016/j.nanoen.2021.106154](https://doi.org/10.1016/j.nanoen.2021.106154).

In Fig. 6, another application domain in the office is demonstrated by

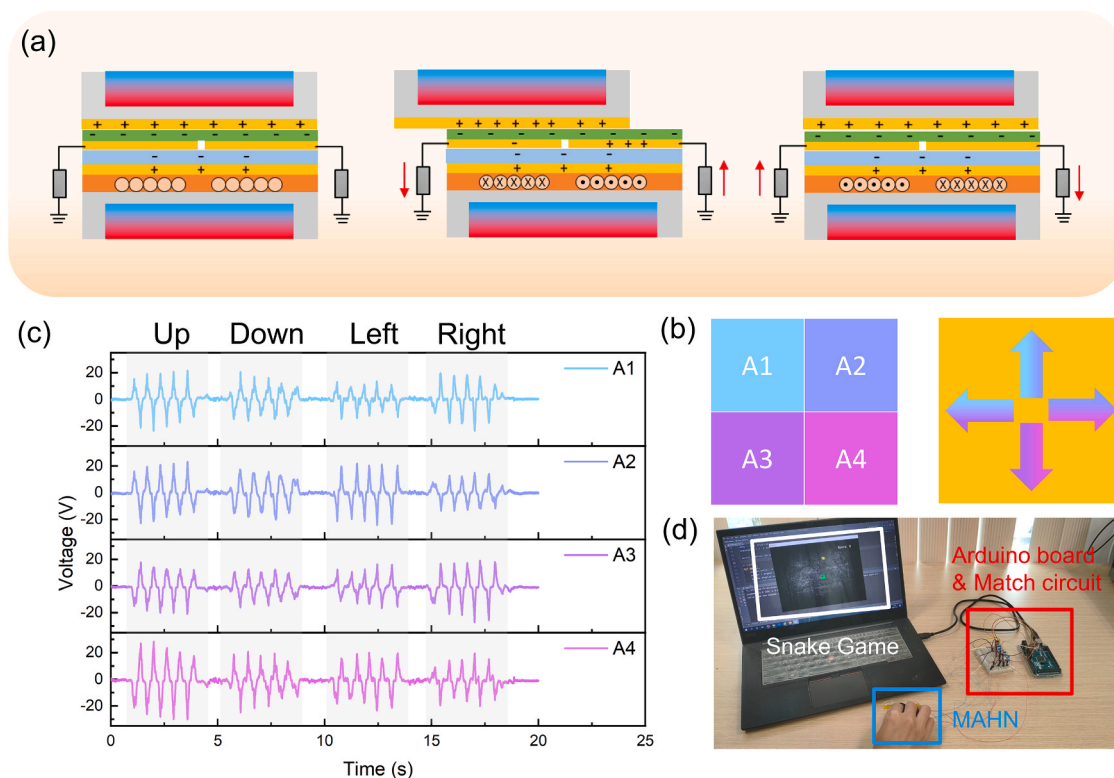


**Fig. 5.** (a) Working principle of the MAHN as a human-machine interface (HMI). (b) Operations designed for the HMI. (c) Output voltages of four electrodes named A1, A2, A3, and A4. (d) Demonstration of "Snake" Game.

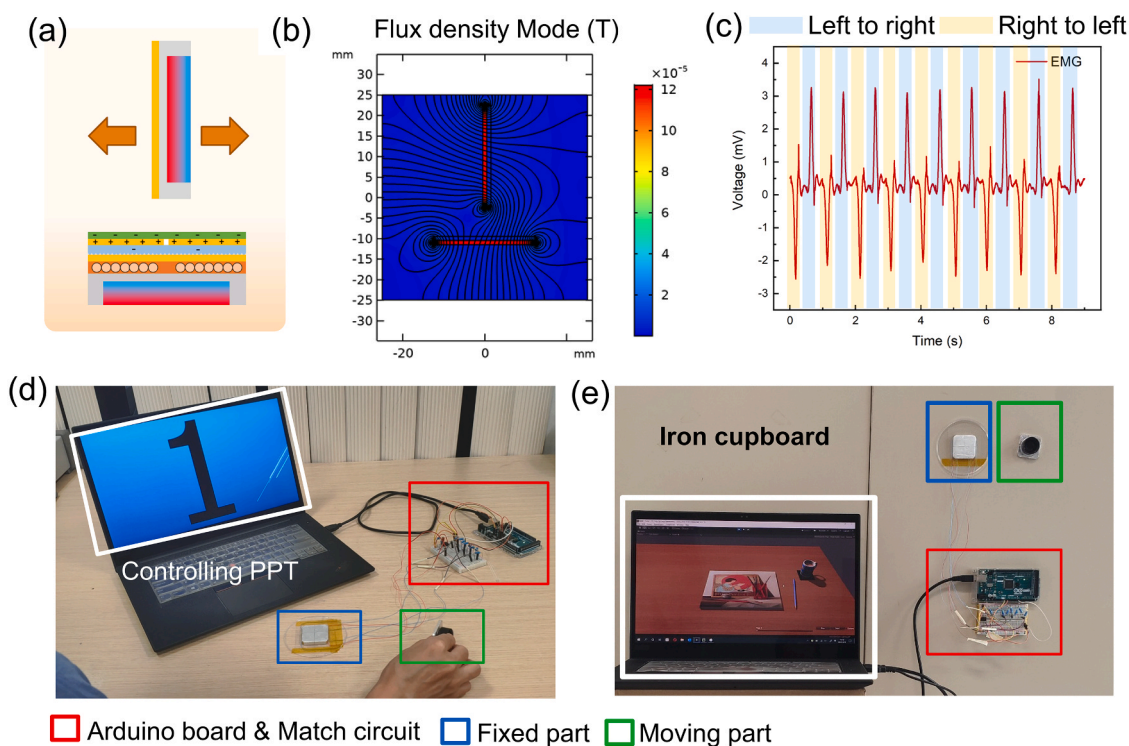


**Fig. 6.** (a) Working principle of the MAHN as a non-contact HMI. (b) Simulated distribution of magnetic field with two orthogonal magnets. (c) Output voltages of EMG unit as the moving part waving above the fixed part. (d) Demonstration of “PPT Controller”. (e) Demonstration of non-contact interactions in the smart home.

applying the MAHN as an advanced human-machine interface. Unlike achieving direction determination with TENGs' signals, the EMG's signals are also introduced to convey motion information. As shown in Figs. 6a and b, basic operations are no-contact typed, which are along with the progressive trend of human-machine interface. Due to the uneven distribution of the magnetic field in two orthogonal placed magnets shown in Fig. 6b, positive peaks and negative peaks will be detected when the vertical moving part drifts over the fixed part. The simulated distribution of the magnetic field is also clarified in Fig. S9, where the positions of vertical magnet influence magnetic induction lines, and correspond moving above the fixed magnet present electric signals' variations in the coil. In Fig. S10, the voltage signals have been decreased as increasing the distance between two parts. As shown in Fig. 6c, the EMG unit in the MAHN has delivered output voltages of 3 mV as the moving part waving with the user's hand above the fixed part about a distance of 10 cm. In the tests, positive peaks are generated when the user waves the vertical moving part from left to right, and negative peaks are generated when the user wave that from right to left. Thus, the obvious difference can be applied to detect the user's simple gesture of waving a hand. Moreover, four electrodes in the TENG part also help to detect when the moving part is off the fixed part. In Fig. S11, output voltages in four electrodes are tested in contact-separation processes, where positive peaks are generated as contacting while negative peaks are generated as separating. The designed operations are summarized in Movie V5, the moving part has been lifted, moved from left to right, moved from right to left, and put down to achieve no-contact moded interactions in HMI.

Supplementary material related to this article can be found online at [doi:10.1016/j.nanoen.2021.106154](https://doi.org/10.1016/j.nanoen.2021.106154).

In the demonstration shown in Fig. 6d and Movie V6, the MAHN has been applied in controlling a PowerPoint document with Arduino 2650, match circuit including operational amplifier circuit, and Python code. Arduino read data is illustrated in Fig. S12, in which designed operations are identified with different signals from the TENG and the EMG. First, when the user lifts the moving part of the MAHN, the document starts

playing with Fullscreen as the Arduino has read out four positive values in four electrodes of the TENGs. Next, operations of the next slide and previous slid of slides have been achieved with the EMG's signal in no-contact mode. Finally, the user can end the presentation by setting the moving part down on the fixed part. The flow chart of interactions is illustrated in Fig. S13. The signals of TENGs are applied to offset the transient unstable EMG's signals and play key roles in determining motions of contact and separation. Besides, the EMG's signals are read through an operational amplifier circuit and applied to distinguish waving directions. Finally, the Arduino sends definite command codes into Python and changes states of presentations. Technically, the MAHN here is played as a commercial laser pointer and realized key functions based on a self-powered sensor. To sum up, the MAHN has shown potential as an advanced human-machine interface both in entertainment and office.

Supplementary material related to this article can be found online at [doi:10.1016/j.nanoen.2021.106154](https://doi.org/10.1016/j.nanoen.2021.106154).

It is worth mentioning that two parts of the MAHN are both magnetic and easily attracted to iron-based furniture and household appliances. In Fig. 6e and Movie V7, two parts of the MAHN can be anywhere on an iron cupboard, similar to refrigerator magnets. A virtual book model is created to demonstrate recognizing simple air gestures in the Smart home. The waving gestures are designed to accord with directions of page-turning. As shown in the demonstration, the user can grab down the moving part and wave it in front of the other part of the MAHN, resulting in page-turning as the user waving hand along the same direction. Likewise, the user can put down the moving part anywhere on an iron cupboard after the above no-contact interactions. Briefly, simple air gestures like waving hands have been recognized by the MAHN.

Supplementary material related to this article can be found online at [doi:10.1016/j.nanoen.2021.106154](https://doi.org/10.1016/j.nanoen.2021.106154).

The array with multiple devices is further developed to illustrated another advanced application in HMI, which is discussed in Fig. 7. As shown in Fig. 7a, a single device of the MAHN needs four channels to be combined into 4 pairs to achieve four kinds of functions. Although four

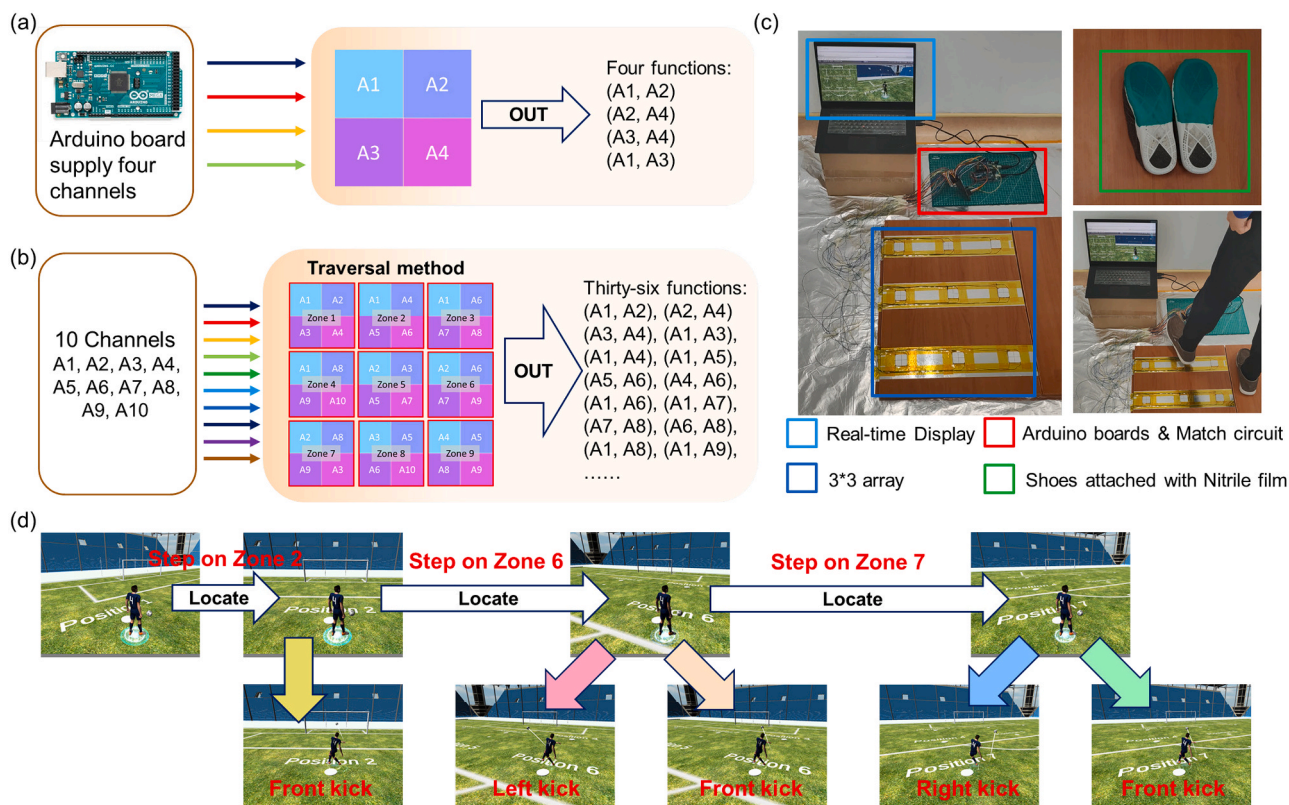


**Fig. 7.** (a) Combination of four channels in the MAHN. (b) Optimization channels by traversal method. (c) Demonstration of a “Football” game. (d) Real-time game display.

channels (A1, A2, A3, A4) can be combined into 6 pairs including (A1, A2), (A1, A3), (A1, A4), (A2, A3), (A2, A4), and (A3, A4), these pairs result in only one kind of combination which satisfies four different pairs in one device. Moreover, in Fig. 7b, the traversal method is applied to find out how many channels are needed to build an array of  $3 \times 3$ . Through calculations in Fig. S14, nine channels generate seven combinations satisfying twenty-eight different pairs in seven devices, ten channels generate nine combinations satisfying thirty-six different pairs in nine devices, and eleven channels generate thirteen combinations satisfying fifty-two different pairs in thirteen devices. As shown in Fig. 7b, ten channels have been labeled in each electrode, but these zones can rotate and switch places. So that, 10 channels are applied to build the array of  $3 \times 3$ , instead of 36 channels counted for thirty-six electrodes. To sum up, nine devices are distinct from each other, and every device presents four kinds of functions like the MAHN in the “Snake” game.

With the channels` optimization, a virtual football game is demonstrated in Fig. 7c and Movie V8. To meet a practical application scenario, outsides of shoes are attached with Nitrile films, and Nitrile films play as the Aluminum film in the above discussed moving part. Similarly, outputs in operations of contact, separation, moving along with different directions are tested and shown in Fig. S15. The magnet in the above-discussed moving part also can be embedded into the insole, and the magnetic attraction between two parts is in favor of the user`s locating at specific points. As shown in Fig. 7d and Fig. S16, when the user puts the foot down on the fixed part of the MAHN, the Arduino board will recognize which zone is the user in. In the demonstration, nine zones of the array and nine positions are in the consistent one-to-one match. When the user steps on “zone 2”, the player in the game locates at “position 2”. Likewise, “position 6” and “position 7” are located when the player completes a successful shooting. The four electrodes in every zone generate different signals when the user does actions of kick forward, kick left, and kick right. At “zone 2”, a successful

shooting has been completed with a front kick. At “zone 6”, the user loses the first try with a left kick, then achieves success with the front kick. Another two attempts at “zone 7” are operated with the right kick and front kick. To sum up, a  $3 \times 3$  array of the MAHN is build and corresponding channels are simplified by traversal method without loss of functions.

Supplementary material related to this article can be found online at [doi:10.1016/j.nanoen.2021.106154](https://doi.org/10.1016/j.nanoen.2021.106154).

### 3. Conclusion

In summary, a magnetic-interaction assisted hybridized triboelectric-electromagnetic nanogenerator is designed and optimized with two magnets in attraction, and a silicone-based cushion with microstructures. The MAHN is based on a contact-separation structured TENG and EMG. And the whole device including a fixed part and a moving part is with a small size of  $35 \text{ mm} \times 35 \text{ mm} \times 8 \text{ mm}$ . At rest state, the moving part and the fixed part are attracted to each other. Outputs of TENG and EMG have been enhanced by the powerful attraction, and the scaling-down effect of output performance by lower operating frequency has been weakened with magnetic attraction induced by the two-magnet design. The MAHN has demonstrated as an efficient hybridized energy harvester for impact energy, as well as a self-powered sensor for the advanced HMI. The TENG delivers the maximum peak power of 6.89 mW at the load of 1.1 M $\Omega$ , and the EMG delivers the maximum peak power of 2.7 mW at the load of 1.1 k $\Omega$ . Benefiting from the designed hybridized buck circuit, outputs of the TENG and the EMG are rectified and integrated to charge different capacitors. Thus, a capacitor of 100  $\mu\text{F}$  is charged to 2.03 V within 30 s, which is better than the performances of individual parts and MAHN with a parallel-connected circuit. A thermometer and a Bluetooth module are powered with different amounts of attracted magnets, implying the high adaptability of the energy harvester. Attributed to the adaptivity of

magnets` amount, the MAHN is applied as an adjustable energy harvester in powering different electronics. Moreover, the intact triboelectric electrode has been cross-divided into four electrodes for applications of the human-machine interface. By utilizing both the triboelectric signals and electromagnetic signals, the MAHN can function as an advanced HMI in entertainment, office, and gaming control, providing higher controlling capability and flexibility in various scenarios. Along with the Arduino platform, the MAHN can transfer moving directions by determining positive peaks in four electrodes, and achieve control like a joystick in a classic game of Snake. Moreover, non-contact operations have been developed by the user waves the vertical moving part above the fixed part, resulting in recognizing simple air gestures for contactless controlling. Combined with contact-separation of the split design, the MAHN helps the user control a PowerPoint document including fullscreen, page down, page up, and end presentation, which realizes most functions of the commercial laser pointer but with a self-powered design. The MAHN also can be easily attached to iron-based furniture and household appliances, similarly to refrigerator magnets, for non-contact interactions in the smart home. Moreover, a  $3 \times 3$  array of the MAHN is prepared and channels are simplified by traversal method without loss of functions to achieve more complex control. Thus, a virtual football game is demonstrated with the Nitrile film attached to the outsole. The user steps on different zones to assist the player in the game in locating at different positions and functions in different zones assist the player in shooting in different directions. Therefore, the hybridized triboelectric-electromagnetic nanogenerator with magnetic interactions is a promising candidate in harvesting distributed mechanical energy and shows great innovation in the HMI.

#### 4. Experimental section

##### 4.1. Fabrication of the magnetic attraction-assisted hybridized triboelectric-electromagnetic nanogenerator (MAHN)

First, two rigid square structures with circular holes are prepared by the 3D printer (ANYCUBIC 4Max Pro) with polylactic acid (PLA). A pair of attracted magnets are respectively attached in the hole with double-sided tape so that two rigid surfaces can be attracted to each other closely. Then a Cu coil with 3800 turns, 24 mm diameter and 1 mm thickness, is fixed in a 3D printed rigid frame with Al tape and attached on the rigid surface of one square part. The other square part is covered with Al tapes.

Second, an Exo-flex 0030 based cushion is prepared by smearing and curing on a commercial conductive textile of 35 mm  $\times$  35 mm. Then the cushion is torn off and flattened on the former rigid frame, where the surface with microstructure is facing the rigid frame.

Third, a square electrode applied for energy harvester and crossed electrodes for the self-powered sensor is fabricated by attaching Al tape on a sheet of FEP film (50  $\mu$ m thickness, 10 cm width, DUPONT). Then the film is flattened on the cushion and fixed with extra parts attached to the rigid margin.

##### 4.2. Characterization and electrical measurement

The outputs data is acquired and saved by Model DSOX3034T Multichannel Oscilloscope (Keysight), where 1000X probes (TT-HVP-15HF) are applied to measure voltage signals of the TENGs, and 1X probe (GTL-101) is applied to measure voltage signals of the EMG. The current signals are measured with Electrometer (Keithley Model 6514) for TENG and low noise current preamplifier (SR570) for EMG. The charging performances are measured by Electrometer (Keithley Model 6514). Optical photos are photoed with OLYMPUS BX53M.

#### CRedit authorship contribution statement

**Long Liu:** Conceptualization, Data curation, Formal analysis,

Investigation, Methodology, Resources, Software, Validation, Visualization, Writing - original draft, Writing - review & editing. **Qiongfeng Shi:** Investigation, Validation, Formal analysis, Visualization, Writing - review & editing. **Zhongda Sun:** Investigation, Validation, Formal analysis, Visualization, Writing - review & editing. **Chengkuo Lee:** Conceptualization, Methodology, Supervision, Project administration, Funding acquisition, Writing - review & editing.

#### Declaration of Competing Interest

The authors declare that they have no known competing financial interests or personal relationships that could have appeared to influence the work reported in this paper.

#### Acknowledgments

This work was partly supported the National Key Research and Development Program of China (Grant No. 2019YFB2004800, Project No. R-2020-S-002) at NUSRI, Suzhou, China; and Singapore-Poland Joint Grant (R-263-000-C91-305) "Chip-Scale MEMS Micro-Spectrometer for Monitoring Harsh Industrial Gases" by Agency for Science, Technology and Research (A\*STAR), Singapore and NAWA "Academic International Partnerships of Wroclaw University of Science and Technology" programmed by Polish National Agency for Academic Exchange Programme.

#### Appendix A. Supporting information

Supplementary data associated with this article can be found in the online version at [doi:10.1016/j.nanoen.2021.106154](https://doi.org/10.1016/j.nanoen.2021.106154).

#### References

- [1] Q. Shi, B. Dong, T. He, Z. Sun, J. Zhu, Z. Zhang, C. Lee, Progress in wearable electronics/photronics—Moving toward the era of artificial intelligence and internet of things, *InfoMat* 2 (2020) 1131–1162, <https://doi.org/10.1002/inf2.12122>.
- [2] F. Wen, T. He, H. Liu, H.-Y. Chen, T. Zhang, C. Lee, Advances in chemical sensing technology for enabling the next-generation self-sustainable integrated wearable system in the IoT era, *Nano Energy* 78 (2020), 105155, <https://doi.org/10.1016/j.nanoen.2020.105155>.
- [3] J. Zhu, M. Zhu, Q. Shi, F. Wen, L. Liu, B. Dong, A. Haroun, Y. Yang, P. Vachon, X. Guo, T. He, C. Lee, Progress in TENG technology—A journey from energy harvesting to nanoenergy and nanosystem, *EcoMat* 2 (2020), <https://doi.org/10.1002/eom2.12058>.
- [4] Q. Shi, T. He, C. Lee, More than energy harvesting – Combining triboelectric nanogenerator and flexible electronics technology for enabling novel micro-/nano-systems, *Nano Energy* 57 (2019) 851–871, <https://doi.org/10.1016/j.nanoen.2019.01.002>.
- [5] B. Chen, Y. Yang, Z.L. Wang, Scavenging wind energy by triboelectric nanogenerators, *Adv. Energy Mater.* 8 (2018), 1702649, <https://doi.org/10.1002/aenm.201702649>.
- [6] Y. Zou, V. Raveendran, J. Chen, Wearable triboelectric nanogenerators for biomechanical energy harvesting, *Nano Energy* 77 (2020), 105303, <https://doi.org/10.1016/j.nanoen.2020.105303>.
- [7] C. Wu, A.C. Wang, W. Ding, H. Guo, Z.L. Wang, Triboelectric nanogenerator: a foundation of the energy for the new era, *Adv. Energy Mater.* 9 (2019), 1802906, <https://doi.org/10.1002/aenm.201802906>.
- [8] P. Carneiro, M.P. Soares dos Santos, A. Rodrigues, J.A.F. Ferreira, J.A.O. Simões, A. T. Marques, A.L. Kholkin, Electromagnetic energy harvesting using magnetic levitation architectures: a review, *Appl. Energy* 260 (2020), 114191, <https://doi.org/10.1016/j.apenergy.2019.114191>.
- [9] H. Liu, J. Zhong, C. Lee, S.-W. Lee, L. Lin, A comprehensive review on piezoelectric energy harvesting technology: materials, mechanisms, and applications, *Appl. Phys. Rev.* 5 (2018), 041306, <https://doi.org/10.1063/1.5074184>.
- [10] P. Bai, G. Zhu, Y. Liu, J. Chen, Q. Jing, W. Yang, J. Ma, G. Zhang, Z.L. Wang, Cylindrical rotating triboelectric nanogenerator, *ACS Nano* 7 (2013) 6361–6366, <https://doi.org/10.1021/nn402491y>.
- [11] H. Zhang, Y. Yang, X. Zhong, Y. Su, Y. Zhou, C. Hu, Z.L. Wang, Single-electrode-based rotating triboelectric nanogenerator for harvesting energy from tires, *ACS Nano* 8 (2014) 680–689, <https://doi.org/10.1021/nn405329z>.
- [12] L. Lin, S. Wang, Y. Xie, Q. Jing, S. Niu, Y. Hu, Z.L. Wang, Segmentally structured disk triboelectric nanogenerator for harvesting rotational mechanical energy, *Nano Lett.* 13 (2013) 2916–2923, <https://doi.org/10.1021/nl4013002>.

- [13] W. Yang, J. Chen, Q. Jing, J. Yang, X. Wen, Y. Su, G. Zhu, P. Bai, Z.L. Wang, 3D stack integrated triboelectric nanogenerator for harvesting vibration energy, *Adv. Funct. Mater.* 24 (2014) 4090–4096, <https://doi.org/10.1002/adfm.201304211>.
- [14] C. Wu, R. Liu, J. Wang, Y. Zi, L. Lin, Z.L. Wang, A spring-based resonance coupling for hugely enhancing the performance of triboelectric nanogenerators for harvesting low-frequency vibration energy, *Nano Energy* 32 (2017) 287–293, <https://doi.org/10.1016/j.nanoen.2016.12.061>.
- [15] X. Xiao, X. Zhang, S. Wang, H. Ouyang, P. Chen, L. Song, H. Yuan, Y. Ji, P. Wang, Z. Li, M. Xu, Z.L. Wang, Honeycomb structure inspired triboelectric nanogenerator for highly effective vibration energy harvesting and self-powered engine condition monitoring, *Adv. Energy Mater.* 9 (2019), 1902460, <https://doi.org/10.1002/aenm.201902460>.
- [16] P. Bai, G. Zhu, Z.H. Lin, Q. Jing, J. Chen, G. Zhang, J. Ma, Z.L. Wang, Integrated multilayered triboelectric nanogenerator for harvesting biomechanical energy from human motions, *ACS Nano* 7 (2013) 3713–3719, <https://doi.org/10.1021/nn4007708>.
- [17] Z. Zhao, C. Yan, Z. Liu, X. Fu, L.M. Peng, Y. Hu, Z. Zheng, Machine-washable textile triboelectric nanogenerators for effective human respiratory monitoring through loom weaving of metallic yarns, *Adv. Mater.* 28 (2016) 10267–10274, <https://doi.org/10.1002/adma.201603679>.
- [18] S. Wang, Y. Xie, S. Niu, L. Lin, Z.L. Wang, Freestanding triboelectric-layer-based nanogenerators for harvesting energy from a moving object or human motion in contact and non-contact modes, *Adv. Mater.* 26 (2014) 2818–2824, <https://doi.org/10.1002/adma.201305303>.
- [19] L. Xu, T. Jiang, P. Lin, J.J. Shao, C. He, W. Zhong, X.Y. Chen, Z.L. Wang, Coupled triboelectric nanogenerator networks for efficient water wave energy harvesting, *ACS Nano* 12 (2018) 1849–1858, <https://doi.org/10.1021/acsnano.7b08674>.
- [20] T. Jiang, L.M. Zhang, X. Chen, C.B. Han, W. Tang, C. Zhang, L. Xu, Z.L. Wang, Structural optimization of triboelectric nanogenerator for harvesting water wave energy, *ACS Nano* 9 (2015) 12562–12572, <https://doi.org/10.1021/acsnano.5b06372>.
- [21] L. Liu, Q. Shi, J.S. Ho, C. Lee, Study of thin film blue energy harvester based on triboelectric nanogenerator and seashore IoT applications, *Nano Energy* 66 (2019), 104167, <https://doi.org/10.1016/j.nanoen.2019.104167>.
- [22] S. Wang, Z.L. Wang, Y. Yang, A one-structure-based hybridized nanogenerator for scavenging mechanical and thermal energies by triboelectric-piezoelectric-pyroelectric effects, *Adv. Mater.* 28 (2016) 2881–2887, <https://doi.org/10.1002/adma.201505684>.
- [23] M. Zhu, Q. Shi, T. He, Z. Yi, Y. Ma, B. Yang, T. Chen, C. Lee, Self-powered and self-functional cotton sock using piezoelectric and triboelectric hybrid mechanism for healthcare and sports monitoring, *ACS Nano* 13 (2019) 1940–1952, <https://doi.org/10.1021/acsnano.8b08329>.
- [24] L. Wang, T. He, Z. Zhang, L. Zhao, C. Lee, G. Luo, Q. Mao, P. Yang, Q. Lin, X. Li, R. Maeda, Z. Jiang, Self-sustained autonomous wireless sensing based on a hybridized TENG and PEG vibration mechanism, *Nano Energy* 80 (2021), 105555, <https://doi.org/10.1016/j.nanoen.2020.105555>.
- [25] K. Zhang, X. Wang, Y. Yang, Z.L. Wang, Hybridized electromagnetic-triboelectric nanogenerator for scavenging biomechanical energy for sustainably powering wearable electronics, *ACS Nano* 9 (2015) 3521–3529, <https://doi.org/10.1021/nn507455f>.
- [26] L. Liu, W. Tang, C. Deng, B. Chen, K. Han, W. Zhong, Z.L. Wang, Self-powered versatile shoes based on hybrid nanogenerators, *Nano Res.* 11 (2018) 3972–3978, <https://doi.org/10.1007/s12274-018-1978-z>.
- [27] Z. Zhang, J. He, T. Wen, C. Zhai, J. Han, J. Mu, W. Jia, B. Zhang, W. Zhang, X. Chou, C. Xue, Magnetically levitated-triboelectric nanogenerator as a self-powered vibration monitoring sensor, *Nano Energy* 33 (2017) 88–97, <https://doi.org/10.1016/j.nanoen.2017.01.031>.
- [28] P. Maharjan, T. Bhatta, H. Cho, X. Hui, C. Park, S. Yoon, M. Salauddin, M. T. Rahman, S. Rana, J.Y. Park, A fully functional universal self-chargeable power module for portable/wearable electronics and self-powered IoT applications, *Adv. Energy Mater.* 10 (2020), 2002782, <https://doi.org/10.1002/aenm.202002782>.
- [29] L. Liu, Q. Shi, C. Lee, A novel hybridized blue energy harvester aiming at all-weather IoT applications, *Nano Energy* 76 (2020), 105052, <https://doi.org/10.1016/j.nanoen.2020.105052>.
- [30] Y. Wu, Q. Zeng, Q. Tang, W. Liu, G. Liu, Y. Zhang, J. Wu, C. Hu, X. Wang, A teeterboard-like hybrid nanogenerator for efficient harvesting of low-frequency ocean wave energy, *Nano Energy* 67 (2020), 104205, <https://doi.org/10.1016/j.nanoen.2019.104205>.
- [31] H. Guo, Z. Wen, Y. Zi, M.-H. Yeh, J. Wang, L. Zhu, C. Hu, Z.L. Wang, A water-proof triboelectric-electromagnetic hybrid generator for energy harvesting in harsh environments, *Adv. Energy Mater.* 6 (2016), 1501593, <https://doi.org/10.1002/aenm.201501593>.
- [32] Z. Wen, H. Guo, Y. Zi, M.H. Yeh, X. Wang, J. Deng, J. Wang, S. Li, C. Hu, L. Zhu, Z. L. Wang, Harvesting broad frequency band blue energy by a triboelectric-electromagnetic hybrid nanogenerator, *ACS Nano* 10 (2016) 6526–6534, <https://doi.org/10.1021/acsnano.6b03293>.
- [33] Y. Zhang, Q. Zeng, Y. Wu, J. Wu, S. Yuan, D. Tan, C. Hu, X. Wang, An ultra-durable windmill-like hybrid nanogenerator for steady and efficient harvesting of low-speed wind energy, *Nano Micro Lett.* 12 (2020) 175, <https://doi.org/10.1007/s40820-020-00513-2>.
- [34] H. Yang, M. Wang, M. Deng, H. Guo, W. Zhang, H. Yang, Y. Xi, X. Li, C. Hu, Z. Wang, A full-packaged rolling triboelectric-electromagnetic hybrid nanogenerator for energy harvesting and building up self-powered wireless systems, *Nano Energy* 56 (2019) 300–306, <https://doi.org/10.1016/j.nanoen.2018.11.043>.
- [35] X. Wang, Z. Wen, H. Guo, C. Wu, X. He, L. Lin, X. Cao, Z.L. Wang, Fully packaged blue energy harvester by hybridizing a rolling triboelectric nanogenerator and an electromagnetic generator, *ACS Nano* 10 (2016) 11369–11376, <https://doi.org/10.1021/acsnano.6b06622>.
- [36] P. Hao, C. Guo, M. Wang, J. Shen, Y. Fu, Two-dimensional triboelectric-electromagnetic hybrid nanogenerator for wave energy harvesting, *Nano Energy* 58 (2019) 147–157, <https://doi.org/10.1016/j.nanoen.2019.01.033>.
- [37] L. Feng, G. Liu, H. Guo, Q. Tang, X. Pu, J. Chen, X. Wang, Y. Xi, C. Hu, Hybridized nanogenerator based on honeycomb-like three electrodes for efficient ocean wave energy harvesting, *Nano Energy* 47 (2018) 217–223, <https://doi.org/10.1016/j.nanoen.2018.02.042>.
- [38] X. Pu, W. Song, M. Liu, C. Sun, C. Du, C. Jiang, X. Huang, D. Zou, W. Hu, Z.L. Wang, Wearable power-textiles by integrating fabric triboelectric nanogenerators and fiber-shaped dye-sensitized solar cells, *Adv. Energy Mater.* 6 (2016), 1601048, <https://doi.org/10.1002/aenm.201601048>.
- [39] L. Zhao, J. Duan, L. Liu, J. Wang, Y. Duan, L. Vaillant-Roca, X. Yang, Q. Tang, Boosting power conversion efficiency by hybrid triboelectric nanogenerator/silicon tandem solar cell toward rain energy harvesting, *Nano Energy* 82 (2021), 105773, <https://doi.org/10.1016/j.nanoen.2021.105773>.
- [40] H. Shao, Z. Wen, P. Cheng, N. Sun, Q. Shen, C. Zhou, M. Peng, Y. Yang, X. Xie, X. Sun, Multifunctional power unit by hybridizing contact-separate triboelectric nanogenerator, electromagnetic generator and solar cell for harvesting blue energy, *Nano Energy* 39 (2017) 608–615, <https://doi.org/10.1016/j.nanoen.2017.07.045>.
- [41] X. Wei, Z. Wen, Y. Liu, N. Zhai, A. Wei, K. Feng, G. Yuan, J. Zhong, Y. Qiang, X. Sun, Hybridized mechanical and solar energy-driven self-powered hydrogen production, *Nano Micro Lett.* 12 (2020) 88, <https://doi.org/10.1007/s40820-020-00422-4>.
- [42] H. Liu, H. Fu, L. Sun, C. Lee, E.M. Yeatman, Hybrid energy harvesting technology: from materials, structural design, system integration to applications, *Renew. Sustain. Energy Rev.* 137 (2021), 110473, <https://doi.org/10.1016/j.rser.2020.110473>.
- [43] T. Zhang, Z. Wen, Y. Liu, Z. Zhang, Y. Xie, X. Sun, Hybridized nanogenerators for multifunctional self-powered sensing: principles, prototypes, and perspectives, *iScience* 23 (2020), 101813, <https://doi.org/10.1016/j.isci.2020.101813>.
- [44] X. Chen, Z. Ren, M. Han, J. Wan, H. Zhang, Hybrid energy cells based on triboelectric nanogenerator: from principle to system, *Nano Energy* 75 (2020), 104980, <https://doi.org/10.1016/j.nanoen.2020.104980>.
- [45] M.-L. Seol, J.-W. Han, S.-J. Park, S.-B. Jeon, Y.-K. Choi, Hybrid energy harvester with simultaneous triboelectric and electromagnetic generation from an embedded floating oscillator in a single package, *Nano Energy* 23 (2016) 50–59, <https://doi.org/10.1016/j.nanoen.2016.03.004>.
- [46] H. Shao, P. Cheng, R. Chen, L. Xie, N. Sun, Q. Shen, X. Chen, Q. Zhu, Y. Zhang, Y. Liu, Z. Wen, X. Sun, Triboelectric-electromagnetic hybrid generator for harvesting blue energy, *Nanomicro Lett.* 10 (2018) 54, <https://doi.org/10.1007/s40820-018-0207-3>.
- [47] M. Zhu, T. He, C. Lee, Technologies toward next generation human machine interfaces: from machine learning enhanced tactile sensing to neuromorphic sensory systems, *Appl. Phys. Rev.* 7 (2020), 031305, <https://doi.org/10.1063/5.0016485>.
- [48] T. Chen, Q. Shi, M. Zhu, T. He, L. Sun, L. Yang, C. Lee, Triboelectric self-powered wearable flexible patch as 3D motion control interface for robotic manipulator, *ACS Nano* 12 (2018) 11561–11571, <https://doi.org/10.1021/acsnano.8b06747>.
- [49] X. Pu, H. Guo, Q. Tang, J. Chen, L. Feng, G. Liu, X. Wang, Y. Xi, C. Hu, Z.L. Wang, Rotation sensing and gesture control of a robot joint via triboelectric quantization sensor, *Nano Energy* 54 (2018) 453–460, <https://doi.org/10.1016/j.nanoen.2018.10.044>.
- [50] W. Choi, I. Yun, J. Jeung, Y.S. Park, S. Cho, D.W. Kim, I.S. Kang, Y. Chung, U. Jeong, Stretchable triboelectric multimodal tactile interface simultaneously recognizing various dynamic body motions, *Nano Energy* 56 (2019) 347–356, <https://doi.org/10.1016/j.nanoen.2018.11.066>.
- [51] F. Wen, Z. Sun, T. He, Q. Shi, M. Zhu, Z. Zhang, L. Li, T. Zhang, C. Lee, Machine learning glove using self-powered conductive superhydrophobic triboelectric textile for gesture recognition in VR/AR applications, *Adv. Sci. (Weinh.)* 7 (2020), 2000261, <https://doi.org/10.1002/advs.202000261>.
- [52] X. Chen, H. Guo, H. Wu, H. Chen, Y. Song, Z. Su, H. Zhang, Hybrid generator based on freestanding magnet as all-direction in-plane energy harvester and vibration sensor, *Nano Energy* 49 (2018) 51–58, <https://doi.org/10.1016/j.nanoen.2018.04.024>.
- [53] J. Wan, H. Wang, L. Miao, X. Chen, Y. Song, H. Guo, C. Xu, Z. Ren, H. Zhang, A flexible hybridized electromagnetic-triboelectric nanogenerator and its application for 3D trajectory sensing, *Nano Energy* 74 (2020), 104878, <https://doi.org/10.1016/j.nanoen.2020.104878>.
- [54] T. Bhatta, P. Maharjan, M. Salauddin, M.T. Rahman, S.M.S. Rana, J.Y. Park, A battery-less arbitrary motion sensing system using magnetic repulsion-based self-powered motion sensors and hybrid nanogenerator, *Adv. Funct. Mater.* 30 (2020), 2003276, <https://doi.org/10.1002/adfm.202003276>.

- [55] F. Xi, Y. Pang, W. Li, T. Jiang, L. Zhang, T. Guo, G. Liu, C. Zhang, Z.L. Wang, Universal power management strategy for triboelectric nanogenerator, *Nano Energy* 37 (2017) 168–176, <https://doi.org/10.1016/j.nanoen.2017.05.027>.
- [56] X. Liang, T. Jiang, G. Liu, T. Xiao, L. Xu, W. Li, F. Xi, C. Zhang, Z.L. Wang, Triboelectric nanogenerator networks integrated with power management module for water wave energy harvesting, *Adv. Funct. Mater.* 29 (2019), 1807241, <https://doi.org/10.1002/adfm.201807241>.
- [57] C. Fang, T. Tong, T. Bu, Y. Cao, S. Xu, Y. Qi, C. Zhang, Overview of power management for triboelectric nanogenerators, *Adv. Intell. Syst.* 2 (2020), 1900129, <https://doi.org/10.1002/aisy.201900129>.



**Long Liu** received his Ph.D. degree from Beijing Institute of Nano energy and Nanosystems, Chinese Academy of Sciences in 2018. He is currently a Research Fellow in the Department of Electrical and Computer Engineering, National University of Singapore. His research interests are focused on energy harvesters and self-powered sensors, wearable electronics, IoT applications in the 5G era.



**Qiongfeng Shi** received his B.Eng. degree from the Department of Electronic Engineering and Information Science, University of Science and Technology of China (USTC) in 2012, and received his Ph.D. degree from the Department of Electrical and Computer Engineering, National University of Singapore (NUS) in 2018. He is currently a Research Fellow in the Department of Electrical and Computer Engineering, National University of Singapore. His research interests include energy harvesters, triboelectric nanogenerators, self-powered sensors, and wearable/implantable electronics.



**Zhongda Sun** Received his B.Eng. degree from the School of Electronic and Information at Soochow University, Suzhou, China, in 2018. After that he received his Master degree from the Department of Electrical and Computer Engineering, NUS, in 2019. He is now a PhD student at the Department of Electrical and Computer Engineering, NUS. His research interests include self-powered wearable sensors and triboelectric nanogenerator.



**Chengkuo Lee** received his Ph.D. degree in Precision Engineering from The University of Tokyo in 1996. Currently, he is the director of Center for Intelligent Sensors and MEMS at National University of Singapore, Singapore. In 2001, he cofounded Asia Pacific Microsystems, Inc., where he was the Vice President. From 2006–2009, he was a Senior Member of the Technical Staff at the Institute of Microelectronics, A-STAR, Singapore. He has contributed to more than 380 peer-reviewed international journal articles. His ORCID is 0000-0002-8886-3649.